Conditions for Core Merging and Planetary Architectures in Inviscid Disks

Noah Goldman

Department of Physics

McGill University, Montreal

March 2023

A thesis submitted to McGill University in partial fulfillment of the requirements of the degree of

Physics

Abstract

Observed exoplanets span a wide range of masses at given orbital periods, with the most common types of planets being super-Earths with masses between $\sim$1–10$M_\oplus$ within orbital periods of $\sim$100 days. Planets are born in disks of gas and solids, and classical theory of disk-planet interaction expects such short-period super-Earths to not exist as they would undergo rapid inward migration and collect at the inner edge of the disk. One way to address this inconsistency between migration theory and exoplanet observations is to consider inviscid disks in which planets are expected to prematurely halt their migration. In this thesis, we explore the orbital dynamics of multi-planetary systems in inviscid disks using N-body code Rebound, resolving the initial short-lived migration, planet-disk and planet-planet interaction, and the final collisional mergers over 100 Myrs. We find that planetary systems that emerge in inviscid disks tend to be more stable against orbital instabilities and that more than 50% of the final system architectures feature intrasystem similarity and mass orderings that have been observed in exoplanetary systems. A smaller fraction of systems show reverse ordering in masses which is not observed in current systems. Whether this is

physical or a consequence of detection bias should be tested with extreme precision radial velocity instruments and upcoming transiting mission PLATO.

Abrégé

Les exoplanètes observées couvrent une large gamme de masses à des périodes orbitales données. Parmi ces planètes, les types les plus courants sont les super-Terres, dont la masse varie entre $\sim$1–10$M_\oplus$ et dont la période orbitale est de $\sim$100 jours. Les planètes naissent dans des disques de gaz et de solides, et la théorie classique de l'interaction disque-planète prévoit que ces super-Terres à courte période n'existeront pas, car elles subiraient une migration rapide vers l'intérieur et s'accumuleraient sur le bord interne du disque. Une façon de résoudre cette incohérence entre la théorie de la migration et les observations d'exoplanètes est de considérer des disques inviscides dans lesquels les planètes devraient arrêter prématurément leur migration. Dans cette thèse, nous explorons la dynamique orbitale des systèmes multi-planétaires dans les disques inviscides en utilisant le code N-body Rebound, résolvant la migration initiale de courte durée, l'interaction planète-disque et planète-planète, et les fusions collisionnelles finales durant 100 millions d'années. Nous constatons que les systèmes planétaires qui émergent dans des disques inviscides ont tendance à être plus stables face aux instabilités orbitales et que plus de 50%

des systèmes présentent une similarité intra-système et des ordres de masse qui ont été observés dans les systèmes exoplanétaires. Une plus petite fraction des systèmes présente un ordre inverse des masses qui n'est pas observé dans les systèmes actuels. Il faudrait vérifier s'il s'agit d'un phénomène physique ou d'une conséquence d'un biais de détection à l'aide d'instruments de vitesse radiale d'une extrême précision et de la mission de transit PLATO à venir.

Acknowledgements

First, I would like to thank my supervisor Dr. Eve Lee for providing me with profound support, guidance, and assistance during my time at McGill, and making possible this project and the knowledge and experience I gained while working on it. Secondly, I extend my thanks to my fellow graduate students at the Trottier Space Institute, as well as the broader TSI community. This work is supported financially by the Trottier Space Institute graduate fellowship. I also acknowledge the Digital Research Alliance of Canada for providing the computational power necessary to run my simulations. Lastly, on a personal note, I extend gratitude to my parents and friends who encouraged me to pursue the M.Sc. Physics program and see it through to the end.

Contribution of Authors

Dr. Eve J. Lee conceived the project. All the numerical simulations and analyses were performed by Noah Goldman under the supervision of Dr. Eve J. Lee. Noah Goldman has authored the majority of the thesis under the direction and guidance of Dr. Eve J. Lee.

Contents

List of Figures

List of Acronyms

AMD Angular Momentum Deficit.

MMSN Minimum Mass Solar Nebula.

Chapter 1

Introduction

1.1 Thesis objective

Migration has formed a common thread in modelling planet formation. One of the early detection of exoplanets was that of a hot Jupiter, a massive planet orbiting very close to their host stars ($\lesssim$0.1 AU; Mayor & Queloz 1995). Given that in our solar system, Jupiter-class objects are found far from the Sun ($\sim$5 AU), a mechanism to bring these planets inward was considered necessary. In fact, disk-planet interaction in classical viscously-accreting disks naturally expects an inward migration of planetary-mass objects (Goldreich & Tremaine, 1980; Lin & Papaloizou, 1993). Ever-growing body of observations motivates improvements to formation models. In viscous disks, disk-induced migration is known to be very rapid, so much so that classic population synthesis models predicted an absence of super-Earth class

objects between ∼0.1 and 1.0 AU (e.g., Ida & Lin, 2008); however, these are found to be the most common types of exoplanets (e.g., Howard et al., 2010; Fressin et al., 2013; Petigura et al., 2013). By contrast, for inviscid disks, the inner disk feedback torque on the planet grows over time, slowing and eventually stopping the latter's migration (e.g., Hourigan & Ward, 1984; Ward, 1997; Yu et al., 2010). The motivation for this thesis is to investigate the orbital dynamics of multi-planetary systems migrating (for a short-distance) in these disks. By estimating the resulting mass and orbital radius distributions and comparing them with that of observed exoplanets, we aim to test the likelihood of planet formation in inviscid disks. We simulate the simultaneous migration of multi-planet systems and their subsequent orbital evolution after the disk dissipates, which advances the current knowledge of planetary dynamics in inviscid disks which has thus far been focused on single or two planet systems in gas-rich environment.

1.2 Thesis organization

This thesis is organized as follows. Chapter 2 provides a summary of relevant scientific literature and the theoretical framework upon which our analyses are built. In particular, we give an overview of the physics behind planetary migration, comparison of migration theory against observations of exoplanets, migration theory in inviscid disks, and planetary core formation. Chapter 3 reviews the methodology of our investigation. We outline how the concepts introduced in Chapter 2 are incorporated and tested in our N-body simulations,

and how we set up the disk and planetary core properties. Chapter 4 presents our results. We describe trends resulting from our simulations including orbital and mass evolution, as well as the frequency and occurence of merging events. In Chapter 5, we describe the possible origins of post-migration drift, criteria for merging events, and mass ordering of our simulated systems. Chapter 6 provides a summary of the text and direction of future study.

Chapter 2

Literature Review

2.1 Migration

Planets are born in spinning disks of gas and dust. Theoretical works of Goldreich & Tremaine (1980) and Lin & Papaloizou (1993) established that the tidal interaction between the planets embedded in these disks and the surrounding gas can lead to rapid inward migration of the planets, potentially giving rise to the short-period planets, including hot Jupiters (Mayor & Queloz, 1995). In this type of migration, called Type I migration, a planet generates spiral waves in the disk gas, and this perturbed gas torques back on the planet. In typical protoplanetary disks, the torque raised in the outer disk wins over that raised in the inner disk, resulting in inward migration of planets.

These torques are maximized where the planet's forcing frequency (in the frame of the

gas) is resonant with the epicyclic frequency (called Lindblad resonance): $(\omega - m\Omega(r))^2 = \kappa^2$ where $\omega \equiv m\Omega_p$ is the forcing frequency in the inertial frame, m is an integer (equivalent to the number of spiral arms; i.e., azimuthal nodes), $\Omega_p \equiv \sqrt{GM_\star/r_p^3}$ is the Keplerian orbital frequency of the planet, G is the gravitational constant, $M_\star$ is the mass of the host star, r_p is the orbital distance of the planet, $\Omega(r)$ is the gas orbital frequency at orbital distance r, and κ is the epicyclic frequency. In particle disks, $\Omega(r)$ would be given by the Keplerian frequency; however, we are dealing with gas disk which is subject to the radial pressure gradient force, and so the gas particles orbit at sub-Keplerian frequency $\Omega(r) = \sqrt{\Omega_k(r)^2 - \eta(c_s/r)^2}$ where $\Omega_k(r) = \sqrt{GM_\star/r^3}$ is the Keplerian orbital frequency, $\eta \equiv d\ln P/d\ln r$ is the dimensionless radial pressure gradient, P is the disk gas pressure, $c_s \equiv \sqrt{kT/\mu m_H}$ is the disk local sound speed, k is the Boltzmann constant, T is the disk temperature, $\mu = 2.37$ is the gas mean molecular weight appropriate for H/He-dominated protoplanetary disk (with solar composition elemental ratios), and m_H is the mass of the hydrogen atom.

The number of peaks of the density perturbation are given by the integer m, and the largest feedback torque on the planet will be given by the perturbed gas closest to the planet which we can locate by taking the limit of $m \to \infty$. In this limit, the site of resonance is reached at $r_L = r_p \pm 2h/3$, where $h = c_s/\Omega_k(r)$ is the disk scale height (see Kley & Nelson, 2012, for a detailed review). This shift in the location of maximal resonance occurs precisely because the gas particles orbit at sub-Keplerian frequency due to gas pressure gradient.

There also exists a corotation torque due to the gas that shares the same orbital frequency of the planet but for the oft-chosen minimum mass solar nebula (MMSN; Hayashi (1981)), the corotation torques cancel out leaving only Lindblad torque contributions to the total resulting in (e.g., Kley & Nelson, 2012)

$$\Gamma^{tot} \approx -2 \left(\frac{M_p}{M_\star}\right)^2 \left(\frac{h}{r_p}\right)^{-2} \Sigma_p r_p^4 \Omega_p^2, \tag{2.1}$$

where M_p is the mass of the planet, and Σ_p is the disk surface density evaluated at r_p. Planetary migration timescale can then be estimated with

$$\begin{aligned} \tau_{migration} &= \left|\frac{r_p}{\dot{r}_p}\right| \\ &= \left|\frac{1}{2}\frac{J_p}{\Gamma^{tot}}\right| \\ &= \left|-0.25\Omega_p^{-1}\frac{M_*}{\Sigma_p r_p^2}\frac{M_*}{M_p}\left(\frac{h}{r_p}\right)^2\right| \end{aligned} \tag{2.2}$$

where J_p denotes the planet's orbital angular momentum. In typical MMSN, the migration timescale is notoriously short, with one Earth mass core at 1 AU ($M_\star = 1M_\odot$, $\Sigma_p = 1700\,\mathrm{g\,cm^{-2}}$, $h/r_p = 0.05$) shuttling to the inner disk within $\sim 10^5$ years (Kley & Nelson, 2012), which is significantly shorter than the typical disk lifetime of a few Myrs measured by Mamajek (2009). It follows that classic theories of migration expect planets to all collect in the inner edge of the disk by the time the disk disappears and the final

planetary systems emerge.

2.2 Migration Theory vs. Exoplanet Observations

Ida & Lin (2008) performed a population synthesis model and found that under Type I migration, super-Earths (planets of mass $1 - 10M_{\oplus}$) within $\sim$1 AU would be uncommon as their migration timescales are too short to allow their formation at those distances.

Transit observations (see, e.g., Dong & Zhu, 2013; Petigura et al., 2013; Fressin et al., 2013) and radial velocity surveys (see, e.g., Howard et al., 2010; Mayor et al., 2011) have shown that exoplanets exhibit a wide range of masses and orbital periods. In particular, super-Earth class exoplanets appear prevalent, accounting for approximately 80% of all the detected planets, and $\sim$30–50% of all Sun-like stars having at least one of these planets within orbital periods of $\sim$300 days. This is in contrast with the findings in Ida & Lin (2008) who predicted such planets to be absent under the influence of classical Type I migration, prompting the need to provide a planetary formation model consistent with both the disk physics that causes migration and with the observed distribution of exoplanets.

While we observe a huge system-to-system variation, the properties of planets within a given system is much more similar to each other (Millholland et al., 2017; Weiss et al., 2018). Millholland et al. (2017) analyzed how the masses and radii for observed planets within a system compare to those in other systems, and find planets to be self-similar in their sizes within a given system compared to those in other systems. As a result, end-to-end formation

models of planets that include disk-planet interaction should additionally account for this intrasystem uniformity.

2.3 Inviscid disk

One suggestion to reconcile the theorized properties of migration with the observed distribution of exoplanets is to use an inviscid disk where the turbulent "viscosity" of the disk gas is so low that gas perturbations cannot be easily diffused away. Before we explain the effect of inviscid disks, we briefly summarize the notion of viscosity in protoplanetary disks. Protoplanetary disks are observed to undergo draining onto the central star, implying a loss of angular momentum. A classic way of removing angular momentum is by viscous diffusion. Since molecular diffusion is too slow to explain the observed lifetimes of protoplanetary disks, this "viscous" diffusion is believed to be mediated by some unknown turbulence which is parameterized with Shakura-Sunyaev parameter α where the kinematic viscosity $\nu \equiv \alpha c_s h$.

Without this diffusion, as planets migrate inward and repel the gas, the gas piles up in the inner orbit while it depletes in the outer orbit until the inner torque completely cancels out the outer torque, prematurely halting the migration of the planet (e.g., Ward, 1997; Rafikov, 2002); in addition, the gaps carved out by the planets can be large and the lack of gas in the vicinity also lowers the total torque on the planet (Kanagawa et al., 2018). Yu et al. (2010) perform hydrodynamic simulations at different values of viscosity and verify migration is

slowed for small planets in inviscid disks by at least an order of magnitude compared to viscous disks. Similarly, Fung & Chiang (2017) performed two-dimensional hydrodynamic simulations of two super-Earth class planets in gas-rich inviscid disks and confirmed the early halting of migration and the ability of the planets to torque the gas towards the star to drive the global disk accretion.

Independent motivation for practically inviscid disks derive from the observed ubiquity of protoplanetary disks showing narrow concentric dust rings even when they are inclined (Pinte et al., 2016) and the observed molecular linewidths (e.g., Flaherty et al., 2017), both of which constrain $\alpha \sim 10^{-4}$, which is about the right order of magnitude for the aforementioned feedback torque to take effect (Fung & Lee, 2018)—this is derived by equating the time it takes for the planet-induced perturbations to become strong enough to torque back on the planet with the time it takes for viscos diffusion to erase away such perturbations, on the scale of the local disk scale height.

With more detailed analytic considerations that resolve the reflection of waves at the outer boundary of the gap carved by the planet, Rafikov (2002) derived an expression for the critical mass of a planet for which migration is expected to shut off at a given location:

$$M_{fb} = 4M_{\oplus} \left(\frac{h/r_p}{0.035} \right)^3 \left(\frac{\Sigma_p r_p^2 / M_\star}{10^{-3}} \right)^{5/13} \tag{2.3}$$

where M_{fb} stands for feedback mass. Through numerical and analytic calculations, Fung &

Lee (2018) found that planets of M_{fb} still travel a short distance inward because it takes some time for the planet-driven perturbation to grow enough to make the net torque on the planet zero. They find the degree of this inward motion to be

$$\frac{\Delta r}{r_{fb}} = -0.5 \left(\frac{\Sigma r_{fb}^2 / M_\star}{10^{-4}} \right)^{4/13}, \tag{2.4}$$

where Σ is the gas surface density, r_{fb} is the orbital radius of the planet when it reaches feedback mass and Δr is the difference between the stopping radius r_f and r_{fb}. Combining equations 2.3 and 2.4, Fung & Lee (2018) derive an expression for r_f, anchored to their simulation parameters:

$$r_f \sim 1\,\mathrm{AU} \left(\frac{1.4 M_{\mathrm{fb}}}{4 M_\oplus} \right) \left(\frac{\Sigma_1}{1700\,\mathrm{g\,cm^{-2}}} \right)^{-5/13} \left[1 - 0.6 \left(\frac{1.4 M_{\mathrm{fb}}}{4 M_\oplus} \right)^{2/13} \left(\frac{\Sigma_1}{1700\,\mathrm{g\,cm^{-2}}} \right)^{42/169} \right] \tag{2.5}$$

where Σ_1 is the gas disk surface density profile evaluated at 1 AU.

Figure 2.1 compares equation 2.5 to the observed exoplanet population, obtained from the NASA Exoplanet Archive (2023). Notably, the predicted mass for a given orbital radius is typically smaller than most of the observed population within ∼1 AU. At larger orbital distances, there exists a significant number of observed planets whose measured masses fall below the predicted mass. These planets could be explained by lower disk gas densities (see Fung & Lee, 2018, their Figure 8) or from the longer dynamical times that can lengthen the time over which plaetary cores can coagulate, although the quantitative

details depend sensitively on a variety of uncertain disk parameters such as the gas surface density, temperature, and the particle size distribution to name a few (see, e.g., Ormel, 2017; Johansen & Lambrechts, 2017, for detailed review on early core formation by pebble accretion). This implies that, at least in the inner orbits, cores must continue increasing in mass after reaching M_{fb}, which can be explained by collisional mergers between initial cores. Much of the motivation for this work is taking this end result from Fung & Lee (2018), and simulating further to encompass the multi-core dynamics and the phase of collisional merger.

2.4 Planetary Core Formation

We have described how planets move around as they interact with the disk gas, but how exactly do planets reach certain mass up to M_{fb} and larger? First, large planetesimals of up to moon-mass objects could emerge from dust-gas instabilities (e.g., Youdin & Goodman, 2005; Chiang & Youdin, 2010; Squire & Hopkins, 2018). These are large enough to trigger pebble accretion, a mode of solid accretion whereby particles of Stokes number order unity can efficiently spiral onto the accreting body due to aerodynamic drag (e.g., Ormel & Klahr, 2010; Lambrechts & Johansen, 2012; Ormel, 2017). Pebble accretion is a self-limiting process. Once the planet becomes massive enough to perturb the surrounding gas and carve out a gap, the planetary torques repel local disk material, creating a pressure maximum exterior to the planet's orbit that prevents pebbles from crossing close to the planet, thus the planet

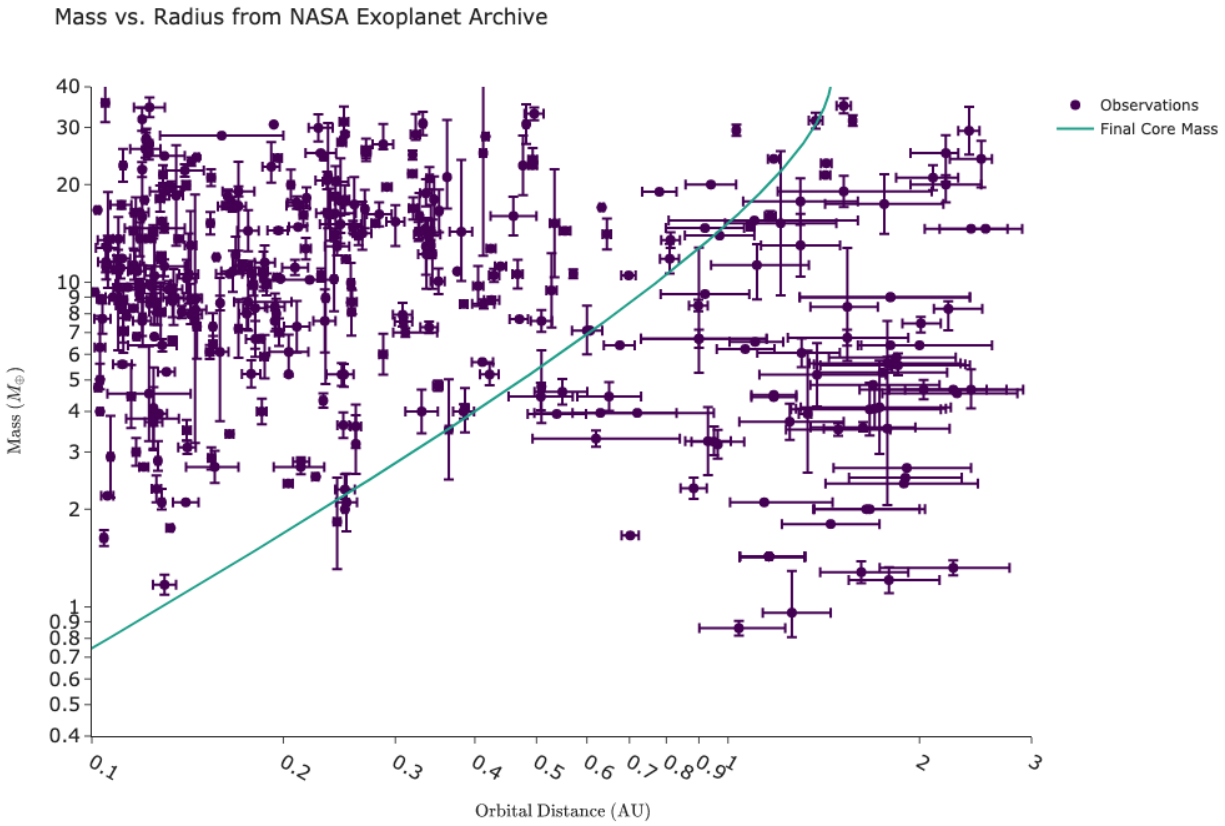

Figure 2.1: Measured masses and orbital distances of published and confirmed planets drawn from NASA Exoplanet Archive (2023) compared to the expected final location vs. planet mass from Fung & Lee (2018), see our equation 2.5. Most planets lie above the expected mass-distance curve from short-lived migration in inviscid disks, suggesting the need for further growth by e.g., collisional mergers.

is isolated from further accretion (Lambrechts et al., 2014). For an inviscid disk, the pebble isolation mass is also a good proxy for the feedback mass as explained by Fung & Lee (2018) as the perturbed gas acts to both trap the pebbles and to cause the feedback effect explained in our Section 2.3.

After reaching the isolation mass, the core can still grow by collisional mergers. Collisions between cores require their orbits to cross, which requires their orbits to gain eccentricity. When embedded in gaseous nebula, the gas dynamical friction damps away the cores' eccentricities, preventing orbit crossings and thus mergers. The eccentricity damping timescale can be calculated by dividing the planet's momentum relative to the gas by the dynamical friction force:

$$\begin{aligned} \tau_{\rm damp} &= \left| \frac{e_p}{\dot{e}_p} \right| \\ &= \left| -0.25 \Omega_p^{-1} \frac{M_\star}{\Sigma_p r_p^2} \frac{M_\star}{M_p} \left(\frac{h}{r_p} \right)^4 \right|, \end{aligned} \tag{2.6}$$

where e_p is the planet's eccentricity. As the disk gas dissipates away and Σ_p drops, $\tau_{\rm damp}$ lengthens and so the dynamical friction has less effect later in the disk lifetime. As a result, core eccentricities can be excited by mutual gravitational perturbations once sufficient time has passed, allowing for orbit mergers, resulting in higher core masses than possible under pebble accretion alone. By comparing the above damping timescale with the orbit crossing timescale empirically determined by Zhou et al. (2007), Lee & Chiang (2016) derived that the

nebular gas needed to be depleted from the solar value by at least four orders of magnitude to trigger merger events. More detailed N-body calculations that account for disk evolution report the required depletion factor to be $\sim 10^3$–10^5 (e.g., Dawson et al., 2016). The exact required depletion factor depends on the spacings between the cores as the orbit crossing timescale is exponentially sensitive to orbital spacings, with cores that are more widely spaced less likely to merge (Zhou et al., 2007; Pu & Wu, 2015).

This giant impact phase is what we simulate in this thesis. What is novel about the work presented here is that we start from the initial conditions set by the initial short-lived migration of multiple cores in inviscid disks. With our simulations, we aim to investigate the final orbital architectures of the multi-planetary systems and compare their properties with the observations.

Chapter 3

Methodology

We use open-source N-body simulation software Rebound (Rein & Liu, 2012) to simulate the orbital dynamics of multiple protoplanetary cores in inviscid disks of which the gas dissipates with time, tracking both the cores' migration as they interact with the gas and the multi-body dynamics once the disk becomes gas-poor. Below we describe how we set up the gas disk and the initial location and masses of the planetary cores, as well as how we incorporate the physics outlined in Chapter 2 to Rebound.

3.1 Disk Parameters

We adopt the minimum mass solar nebula (MMSN; Hayashi (1981)) as the disk gas surface density profile, modified for exponential dissipation

$$\Sigma(r) = 1700 \text{ g cm}^{-2} \left(\frac{r}{1 \text{ AU}}\right)^{-3/2} e^{-\frac{t}{\tau_{\text{diss}}}}, \tag{3.1}$$

where r is the orbital distance, t is time, and τ_{diss} is the characteristic disk lifetime that we vary between 0.5 and 1 Myr, motivated by the observed disk lifetime of ∼Myr measured by Mamajek (2009).

The temperature at the disk midplane is assumed to be set purely by the irradiation from the central star. Accounting for the flaring of the disk due to the vertical hydrostatic equilibrium, we have

$$T(r) = 1000 \text{ K} \left(\frac{r}{0.1 \text{ AU}}\right)^{-3/7}, \tag{3.2}$$

following Chiang & Goldreich (1997).

With the temperature profile, we can define the vertical scale height of the disk (computed from the vertical hydrostatic equilibrium $h = c_s/\Omega$) and therefore the disk aspect ratio:

$$\frac{h}{r} = 0.038 \left(\frac{r}{\text{AU}}\right)^{2/7} \left(\frac{M_\star}{M_\odot}\right)^{-1/2}. \tag{3.3}$$

3.2 Initial Condition of Planets

Each run simulates a system of six cores migrating simultaneously, with initially circular and coplanar orbits. The initial location of cores is determined by the orbital radius of the innermost core, and the prescribed spacing between the cores. The innermost core always begins at 1 AU as a reference. Each successive core begins at an orbital radius of the inner adjacent core, plus a spacing parameter. The spacing for a given run is a scalar multiple of a local disk scale height h. Dong & Fung (2017) determined the size of disk gaps cleared by single cores based on orbital distance and mass and found gaps of $\sim 2-8h$. Migrating cores must be spaced such that each can clear its own gap. As our goal is to bound the range of spacings that allow for core merging, we choose values between $2h$ and $4h$ with resolution $0.4h$. Based on initial experimentation, our choice of spacing gives the lower and the upper limit on the spacings that allow merging events within the simulation time of 100 Myrs.

Our simulation begins from the initial short-lived migration in inviscid disks once the cores have already completed their pebble accretion and so we set the initial core mass to M_{fb} (see equation 2.3). To detect when collisions occur, we need to estimate the physical size of our cores. We assume core density is equal to bulk Earth density, and thus each core's physical radius scales with its mass as

$$R_p = R_\oplus \left(\frac{M_p}{M_\oplus}\right)^{1/3}, \tag{3.4}$$

where R_p represents the core's physical radius.

3.3 Disk-Planet Interaction

We implement the migration and the eccentricity damping of cores through exponential decay with e-folding timescale set by equation 2.2 and equation 2.6, respectively:

$$r_p = r_p(t=0)e^{-t/\tau_{\rm migration}}; \tag{3.5}$$

$$e_p = e_p(t=0)e^{-t/\tau_{\rm damp}}. \tag{3.6}$$

using the disk properties outlined in Section 3.1, evaluating the time-evolving Σ at each timestep. More precisely, we add an extra force to the usual N-body dynamical effects so that cores, once orbit-averaged, produce exponential decay in r_p and e_p; the numerical details of applying these extra forces can be found in Tamayo et al. (2020a). We stop the migration when the planet reaches a radius r_f (equation 2.5) since at this poin, the net Lindblad torque is zero, but we do not shut off eccentricity damping since this damping is due to one-sided Lindblad torque which is non-zero. Even when the disk gas practically disappears, the gravitational interaction between cores (e.g., secular interaction; Pu & Lai 2019) can cause their inward drift, in addition to an increase in eccentricity.

3.4 Planet-Planet Interaction

Our simulation is concerned with both migration and core collisions. At any time throughout the simulation, a pair of cores collides if the distance between the core centers is less than the radii of the respective cores. The collision is then resolved by merging the two cores with the mass, size, and orbital properties of the new core set by conserving momentum, mass, and volume. Quantities indirectly assigned to cores such as $r_f, \frac{\dot{r}_p}{r_p}, \frac{\dot{e}_p}{e_p}$, are not reassigned to merged cores as all our merger events take place long after migration and disk depletion, and thus these quantities are no longer relevant to the motions of the cores.

For each pair of dissipation time and core spacing, we run 100 simulations, identical except for the true anomaly of each core in each system, which is drawn randomly between 0 and 2π on a linear scale. Simulations were run for 100 Myr. Resulting data were output to text files including orbital radii, eccentricity, and mass of each core at time intervals of around 10 kyr for each run.

Chapter 4

Results

4.1 Orbital Evolution of Cores

Figure 4.1 illustrates the overall orbital evolution of the cores we simulate. We see a rapid inward migration for all the cores at $\sim 10^4$–10^5 years which is short-lived due to a combination of disk gas depletion and also the cores' arrival at their r_f. The cores do not completely stop at r_f however, and we observe a small drifting in likely due to their secular interaction with each other. For cores that are tightly spaced ($2.0h$; left panels), we find that the cores readily merge at $\sim 10^6$ yrs. The degree of dynamical inward drift after the halting of disk-induced migration is shown in Figure 4.2. While the degree of inward drift is not too dramatic (typically only about $\sim$20%), we observe a general trend of stronger drift for more widely-spaced planets. There is no visible dependence of the degree of this inward drift on

the disk dissipation timescale (left and right panels of Figure 4.2), suggesting the drift is dynamical in origin. In fact, we have ran a test case of a single core undergoing Type I migration until it reaches r_f and in that case, we did not see any further inward drift.

4.2 Orbital Architectures and Merger Events

To quantify the likelihood of a core merger, we plot the histogram of the number of cores (core multiplicity) in each system at the end of the simulation, as shown in Figure 4.3. At one extreme (e.g., cores separated by $4h$), all runs result in a multiplicity of six, and thus no merger occurred, and at the other extreme (e.g., cores separated by $2h$), we see just two cores remaining, indicating nearly all the original cores merged into a pair. More typically, we see a post-merger multiplicity of 3. As one may expect, as core spacing increases, so does the core multiplicity. One interesting observation is that none of our simulations end up with 5 cores, suggesting how if there is a merger, it will always trigger at least one another merger.

As an example, Figure 4.4 illustrates the evolution of masses and orbital distances of cores in one of the simulations with disk dissipation time of 0.5 Myrs and initial orbital spacing of $2.0h$. From the multiplicity histogram, $\sim$90% of the runs for this pair of parameters result in at least one merger event. As can be seen in Figure 4.4, cores 1 and 2, 3 and 4, 5 and 6 merge during the simulation, amounting to a final 3 cores in the end. These mergers occur long after cores reach their final orbital radii, when the disk gas is significantly depleted, as

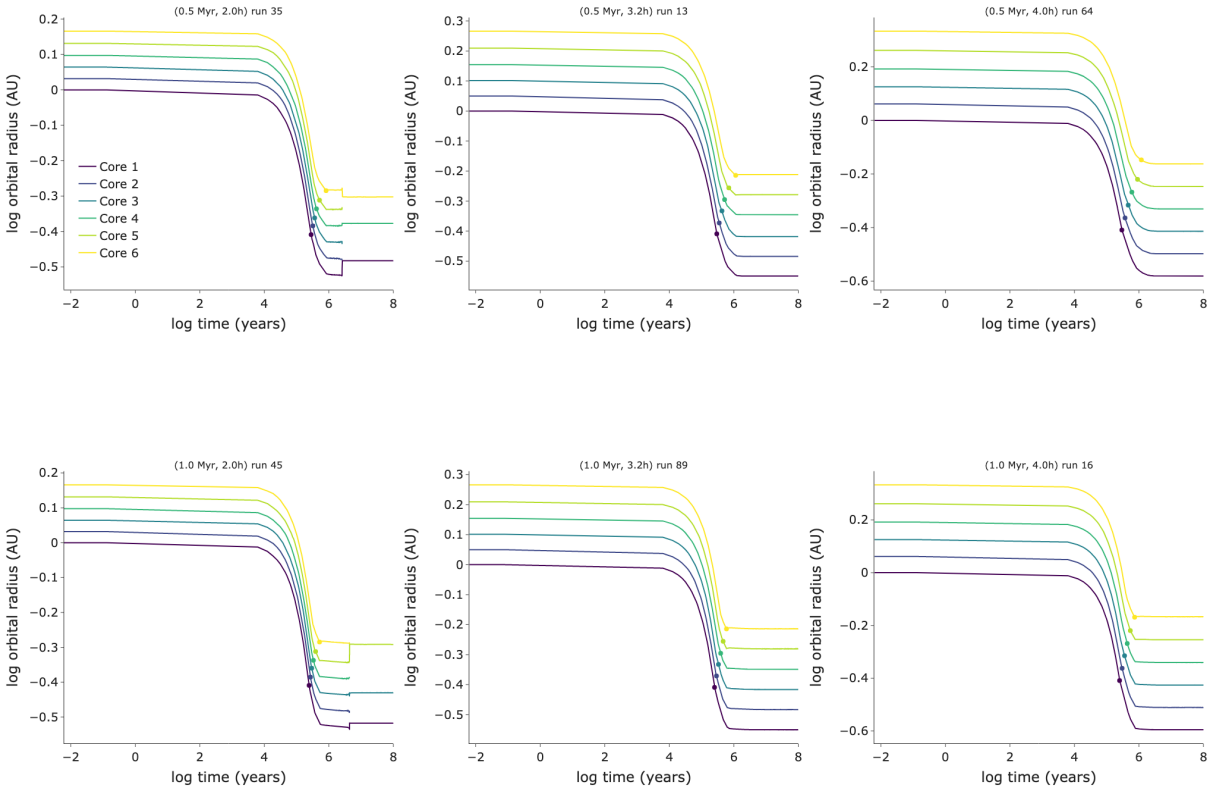

Figure 4.1: The orbital evolution of cores from the start to the end of our simulations. Top panels illustrate disk gas depletion timescale of 0.5 Myrs while the bottom panels show gas depletion timescale of 1 Myr. The runs in the left panels have initial orbital spacing of $2h$; the middle panels $3.2h$; and the right panels $4.0h$. For each track, we indicate with circles when the core reaches its r_f. Even after the cores reach their expected stopping radius, they still move inward, with the innermost planet drifting in the farthest. We see that the cores readily merge when they are tightly spaced.

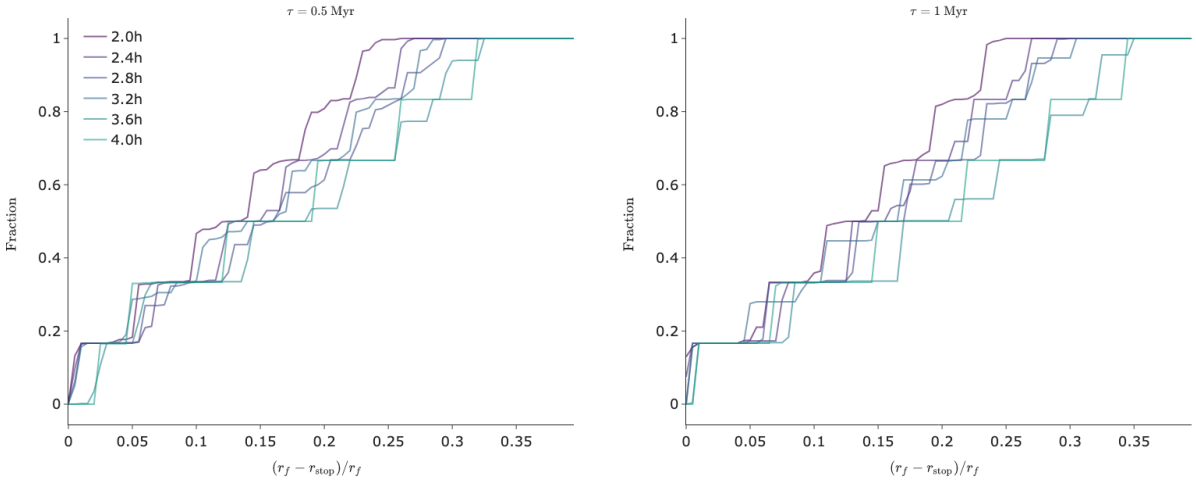

Figure 4.2: The cumulative distribution of $(r_f - r_{\rm stop})/r_f$ where $r_{\rm stop}$ is the final stopping distance after the dynamical inward drift, measured at $\sim$2 Myr. Disk dissipation time of 0.5 Myrs and 1.0 Myrs are shown in the left and right panels, respectively. The degree of inward drift is generally mild, but is slightly more pronounced for more sparsely-spaced systems.

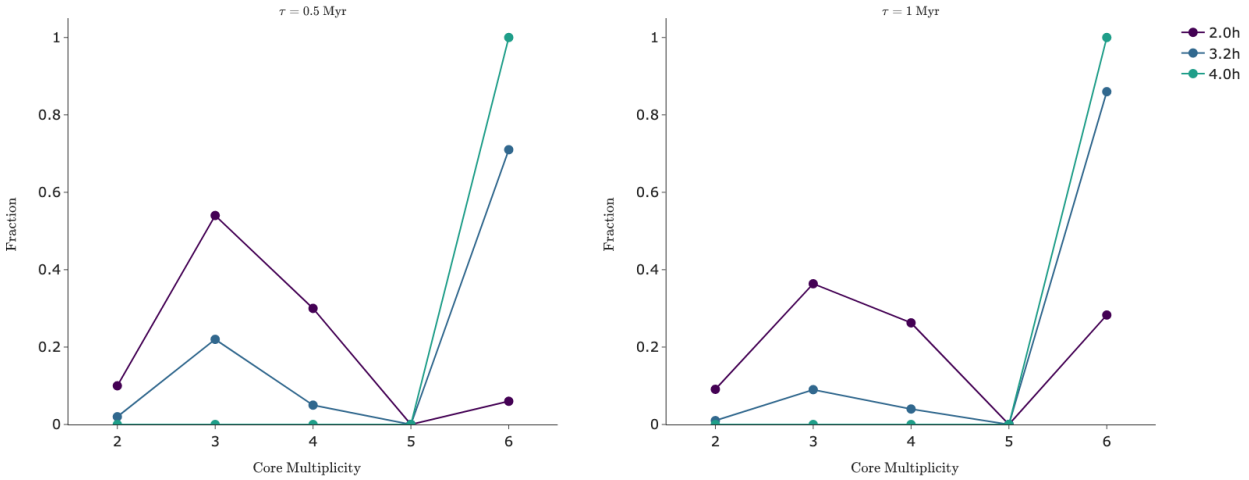

Figure 4.3: Histogram of core multiplicity for different initial orbital spacing. The left and the right panel each illustrates the results of simulations with disk dissipation timescale 0.5 Myrs and 1.0 Myr, respectively. In general, we find mergers to more likely occur when cores are tightly spaced, and we see no merger event for initial spacing of $4h$.

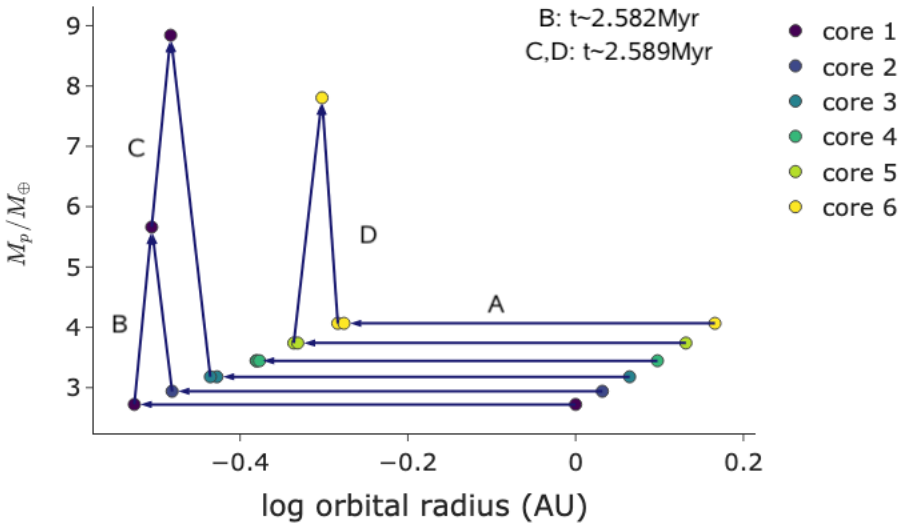

Figure 4.4: Evolution over mass vs. orbital distance plane for $\tau_{\rm diss} = 0.5$Myrs and orbital spacing of $2.0h$ of a specific realization. The path A tracks the initial disk-induced migration and tracks B, C, and D denote the post-migration merger events. Mergers are more likely to occur in the inner disk due to shorter dynamical time and for this realization, we find the final mass of the inner planet to be larger than the outer planets.

expected.

A striking feature of Figure 4.4 is that the innermost cores are the most massive due to successive mergers there over short timescales. While mergers are expected to occur most likely in the innermost orbits, in typical exoplanetary systems, planetary masses tend to increase toward longer orbital periods (Millholland et al., 2017). Following Millholland et al.

(2017), we define a mass ordering parameter

$$\mathcal{O}_M \equiv \sum_{\substack{i=1 \\ P_i<P_{i+1}}}^{N_{\rm pl}-1} \log \frac{M_{p,i+1}}{M_{p,i}} \tag{4.1}$$

where $N_{\rm pl}$ is the number of planets in a given system, P_i is the orbital period of the i-th core, and $M_{p,i}$ is the mass of the i-th core. Our initial protocores have $\mathcal{O}_M > 0$ as $M_{\rm fb}$ are larger at longer orbital periods. The cumulative distributions of $\mathcal{O}_M$ illustrated in Figure 4.5 demonstrate that merger events tend to flatten and sometimes reverse the mass ordering in a given system, driving $\mathcal{O}_M$ closer to zero and sometimes negative. We still see more than 50% of the systems remain forward-ordered with $\mathcal{O}_M \geq 0$ in agreement with observed exoplanetary systems. Systems that are initially more widely spaced ($\gtrsim 3h$) tend to maintain their initial $\mathcal{O}_M$ reflecting the rarity of core mergers in these systems, in alignment with Figure 4.3.

The positive mass ordering can also be seen in Figure 4.6 which demonstrates how the typical core masses generally rise towards larger orbital distances. At 0.2–0.25 AU, we see that all the cores retain their initial, pre-merger mass; this is the innermost edge of the planetary systems that we simulate and so should the cores exist here, they are part of the systems that were so stable that they never underwent any merger process over 100 Myrs. The range of core masses we obtain in our simulations are considerably narrower than what we see in the observations. We expect to obtain a broader range of masses if we vary the disk

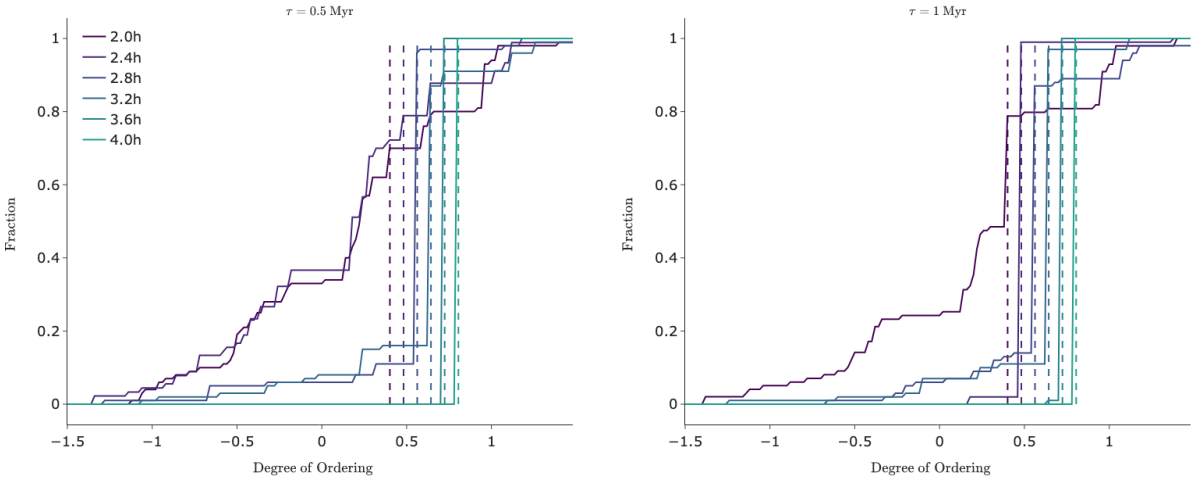

Figure 4.5: Cumulative distribution function of the mass ordering function $\mathcal{O}_M$ calculated over the simulated systems. Disk dissipation time of 0.5 Myrs and 1.0 Myrs are shown in the left and right panel, respectively. Vertical dotted lines represent initial ordering based on M_{fb} before any mergers occur. When spacings allow for mergers, $\mathcal{O}_M$ is driven towards $\lesssim$0 and we find that systems are often reverse ordered, while many remain forward ordered.

properties such as the gas surface density and the temperature profile which will change the initial masses of the protocores $M_{\rm fb}$ (see equation 2.3), but reproducing the entire population of observed exoplanetary systems is beyond the scope of this thesis.

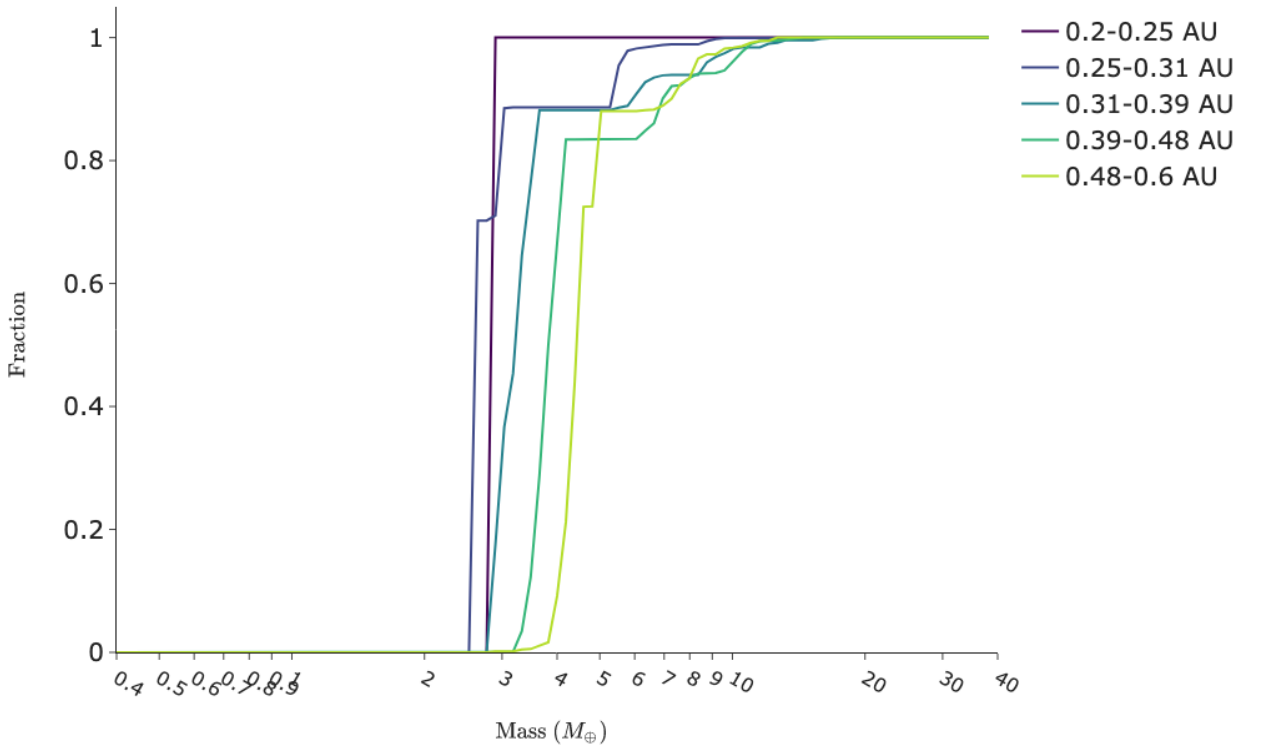

Figure 4.6: Cumulative distribution function of final core masses for different ranges of final orbital distances, evaluated over all simulations. Overall, masses tend to increase at larger orbital distances. We see an exception between 0.2–0.25 AU vs. 0.25–0.31 AU; we see those found between 0.2 and 0.25 AU to retain its original mass as these derive from systems that remained stable over 100 Myrs.

Chapter 5

Discussion

5.1 Origin of the Post-Migration Drift

One surprising result from our calculation is that the cores undergo an inward drift of $(r_f - r_{\rm stop})/r_f \lesssim 20\%$ after their disk-induced migration is complete and when the disk gas is on the verge of complete dissipation (see Figure 4.2). Such a drift is not observed in a single core system, suggesting that the dynamical interaction between multiple cores may be the cause. Our systems are not deliberately placed in mean motion resonance so the dynamical interaction is likely secular in nature which does not modify the orbital energies. It follows that the conserved quantity in such a problem is the angular momentum deficit (AMD), defined as the deficit in total angular momentum in the system as compared to that of a

coplanar and circular system (e.g., Laskar, 1997):

$$\Lambda = (GM_\star)^{1/2} \sum_{i=1}^{N_p} M_{p,i}\sqrt{r_i}[1 - \sqrt{1 - e_i^2}] \tag{5.1}$$

where N_p is the number of cores in the system and $M_{p,i}$ is the mass of the i-th core, r_i is the orbital distance of the i-th core, and e_i is the eccentricity of the i-th core. In writing Λ, we have assumed coplanar systems as we do not vary inclination in any of our simulations. We can define the minimum AMD required for the innermost core to drift to $r_{1,\mathrm{stop}}$ from $r_{1,\mathrm{f}}$ and solve for the required rms eccentricity of the outer neighboring cores to reach this AMD (Petrovich et al., 2019):

$$e_{\mathrm{rms}}^2 \sim \frac{2(1 - \sqrt{r_{1,\mathrm{stop}}/r_{1,\mathrm{f}}})}{\sum_{i=1}^{N_p} \frac{M_i}{M_1}\sqrt{r_{\mathrm{i,f}}/r_{1,\mathrm{f}}}}. \tag{5.2}$$

In Figure 5.1 we show that under the secular theory, the rms eccentricities of the outer cores need to be ∼0.08, ∼0.16, ∼0.20 to cause an inward drift of the innermost core at the level of 5%, 20%, and 30%, each corresponding to roughly 20, 50, and 80 percentile of the distribution of inward drift observed in all our simulations (see Figure 4.2). Comparing this required eccentricity to the measured eccentricities in our simulated systems prior to merger evaluated at 2 Myr, we find that typical systems are rather dynamically cold with maximum eccentricity only at the level of ∼0.01 (see Figure 5.2). Comparing the left and the right panel of Figure 5.2, we see that the effect of gas eccentricity damping is acute prior to merger as the eccentricities are significantly smaller for gas dissipation timescale of 1 Myr

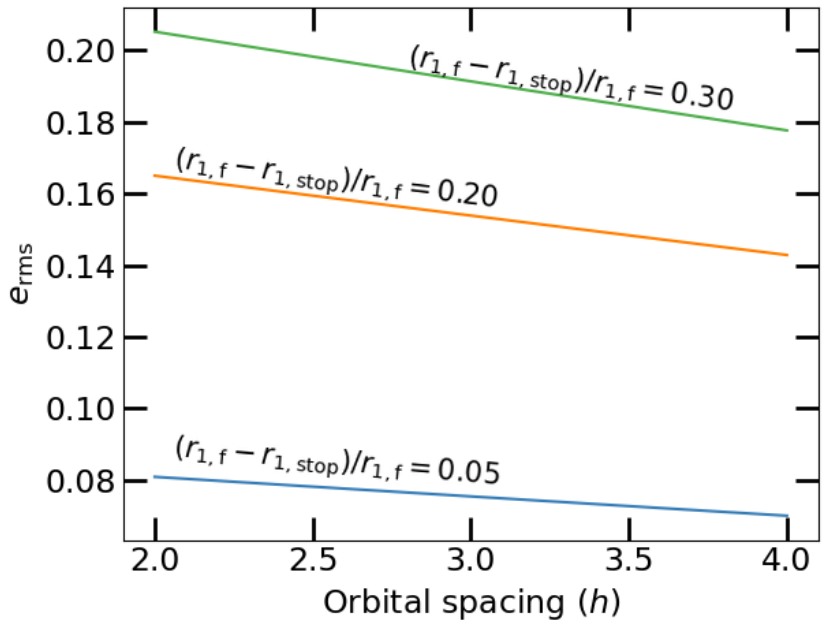

Figure 5.1: The required rms eccentricity $e_{\rm rms}$ of outer cores to cause the innermost core's inward drift at the level of 5, 20, and 30%, each corresponding roughly to 20, 50, and 80 percentile of overall inward drift rates as illustrated in Figure 4.2. There is a slight decrease in $e_{\rm rms}$ at larger initial orbital spacing due to a slightly larger denominator in equation 5.2.

as compared to 0.5 Myr. The existence of dissipative effects implies a strict application of secular theory may be incorrect. More careful analysis of detailed orbital dynamics (e.g,. Pu & Lai, 2019) accounting for disk-planet interaction would be required to definitively identify the origin of the post-migration drift, which is a subject of future work.

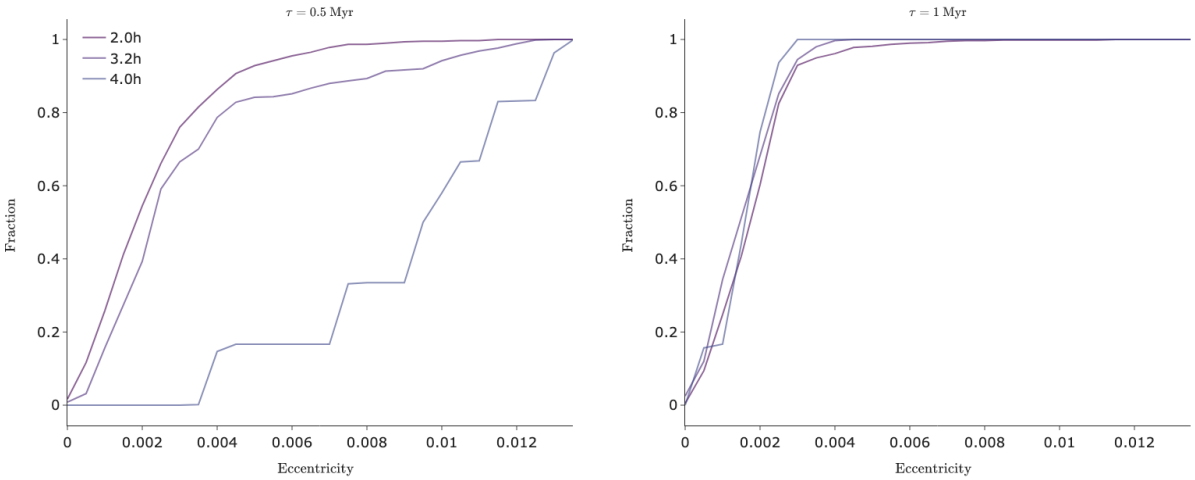

Figure 5.2: The cumulative distribution of core eccentricity e_p, measured at $\sim$2 Myr. Disk dissipation time of 0.5 Myrs and 1.0 Myrs are shown in the left and the right panel, respectively. With shorter disk dissipation time, eccentricities are more likely to be higher in general, and are more likely to be higher at wider spacings. At $\tau_{diss} = 1$Myr, eccentricity distributions are consistent for different spacings, implying that the disk damping effects remain active at $\sim$2 Myr.

5.2 Criteria for Merging

Our N-body results suggest that core mergers are generally rare events unless they are initially spaced apart by $\lesssim 3h$. We have chosen h as our unit of spacing as these are the natural spacing of gaps carved out by massive planets as they repel the nebular gas in their vicinity (Dong & Fung, 2017). However, the natural unit of orbital dynamics is the mutual Hill radius defined as

$$r_{\rm mH} = \left(\frac{m_1 + m_2}{3M_\star}\right)^{1/3} \frac{r_1 + r_2}{2} \tag{5.3}$$

where m_1 and m_2 are the masses of the inner and the outer planets in an adjacent pair, and r_1 and r_2 their orbital distances. Defining the orbital spacing $k = \Delta a / r_{\rm mH}$, Pu & Wu (2015) derived an expression for the survival probability (i.e., the probability for the multi-planetary systems to *not* undergo any merger event):

$$s(k_{\rm eff}, \tau) = \begin{cases} 1 - \exp\left[-\left(0.5k_{\rm eff} - 0.6 - 0.35\log_{10}\tau\right)^2\right], & k_{\rm eff} \geq 1.2 + 0.7\log_{10}\tau \\ 0, & k_{\rm eff} < 1.2 + 0.7\log_{10}\tau \end{cases} \tag{5.4}$$

where $k_{\rm eff} = \langle k \rangle - 0.5\sigma_k$, $\langle k \rangle$ is the mean k in a given system and σ_k its standard deviation, $\tau = t/P_1$, t is the time at which the survival probability is measured (i.e., the age of the system), and P_1 is the orbital period of the innermost planet. More accurately, τ is the physical timescale divided by the first encounter time, which usually occurs at closest-in orbits where dynamical timescales are short. For a system of 7 planets, $k_{\rm eff} \lesssim 7.3$ would

spell orbital instability and a merger event by 100 Myr with ∼100% probability (see Pu & Wu, 2015, their Figure 2).

In Figure 5.3, we recast the spacings between our six simulated cores in terms of mutual Hill radius. We see that for all our simulations, the orbital spacing is always below 7.3 mutual Hill radii. It is thus surprising that we find mergers to be so rare. It could be that our smaller initial multiplicity lowers the $k_{\rm eff}$ required for mergers as higher multiplicity makes a system more unstable (see also Funk et al., 2010). Another difference between our study and Pu & Wu (2015) is that we have cores that are different in masses within a given system, with the mass steeply rising at larger orbital distances effectively decreasing the Hill spacing there (for a fixed h-spacing). The non-uniform mass and spacing could be affecting the dynamical stability of the systems. It may be that the first encounter time is not to be evaluated at the closest-in orbit but farther out, which would decrease the critical $k_{\rm eff}$ at which the mergers are guaranteed to occur. Testing against the open-source machine-learning prediction suite of orbital stability SPOCK (Tamayo et al., 2020b), we find that these systems have no chance of being stable over 100 Myrs. All aforementioned studies of orbital dynamics assume a completely gas-free environment, so we conjecture that the residual remaining gas in our simulation still acts to continuously damp away some level of core eccentricities, making all our systems more resilient against merging events. However, similar N-body simulations that account for eccentricity damping with outwardly increasing initial core mass found such tightly-spaced systems to be easily prone to orbital instability (Dawson et al., 2016) so it

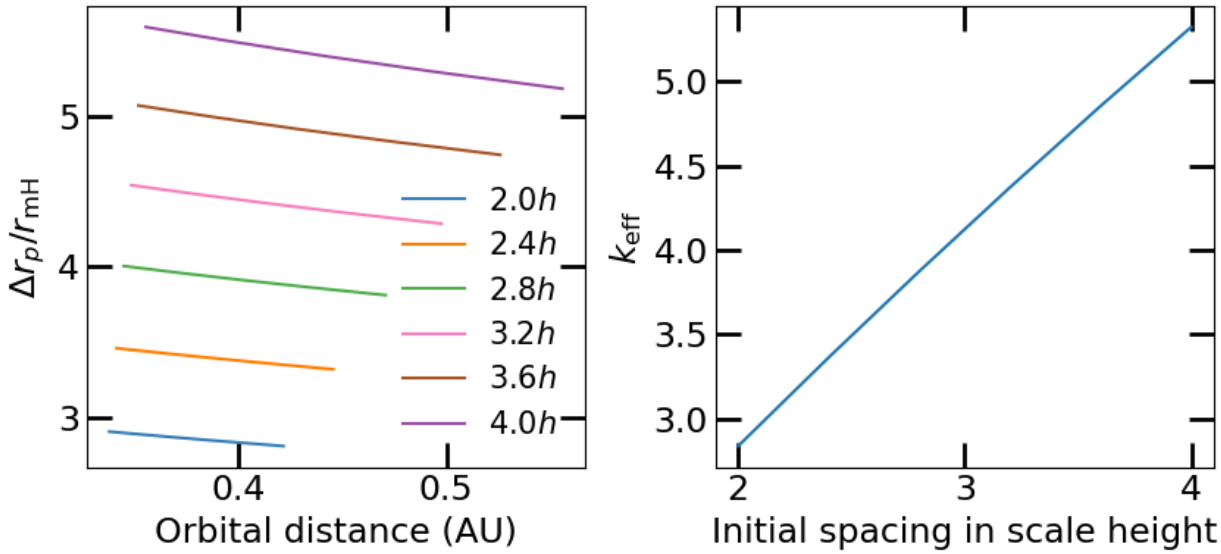

Figure 5.3: Left: expected orbital spacing in terms of mutual Hill radii for each initial disk scale height spacing. Right: the effective Hill spacing $k_{\rm eff}$ for the initial spacing in disk gas scale height. All of our simulations predict $k_{\rm eff}$ small enough compared to the critical spacing of $\sim$7 given by Pu & Wu (2015) that they should have all undergone orbital instability and collisional mergers.

remains unclear why exactly our simulation setups lead to more stable systems. A more systematic study that gradually introduce complications (i.e., increased number of cores, uniform Hill spacing vs. uniform h-spacing, uniform mass vs. outwardly increasing mass, gas damping vs. no damping) would be required to answer this question, which is a subject of future work.

5.3 Mass Ordering in Inviscid Disks

In inviscid disks, the initial protocore mass vs. orbital distance expected from pebble accretion and disk feedback torque is steep, with masses falling below $\sim$1–2$M_\oplus$ within $\sim$0.3 AU (see Figure 2.1). As shown in Figure 2.1, in the observed planetary systems, short-period planets are measured to have masses well above $\sim 2M_\oplus$. Furthermore, given planetary systems are known to feature relative similarity in both radius (Weiss et al., 2018) and mass (Millholland et al., 2017) among the constituent planets. Previously, this intrasystem similarity has been thought to disfavor the formation of planetary cores via post-disk merger processes due to the latter's stochastic nature. However, the fact that mergers occur in the innermost periods first and that in most initial protocore formation scenario, the innermost cores are the least massive suggest that collisional mergers would lead to more self-similar systems. Recent N-body simulations that start with initial protocore properties expected from planetesimal accretion have indeed demonstrated that such intrasystem similarity is a natural outcome of post-disk merger processes (MacDonald et al., 2020).

We arrive at similar results with the initial conditions that are specific to protocore formation in inviscid disks, which lead to the initial mass vs. orbital distance that is steeper than that adopted by MacDonald et al. (2020). Typically, our systems have $\mathcal{O}_M \sim 0.2$–0.5 (Figure 4.5), which is similar to what is measured in the observed exoplanetary systems (see Figure 8 of Mishra et al., 2023). We also find $\lesssim$50% of all our realizations ending up with

reverse mass order $\mathcal{O}_M$ which is not seen in the observations, although the detection bias against small planets at longer orbital periods imply that we cannot rule out the existence of such systems, albeit likely rare. Following up on known systems with extreme precision radial velocity instruments that can probe lower mass planets at longer orbital periods as well as PLATO that promises to probe down to an Earth-size planets beyond $\sim$100 days should be able to determine both the existence and the occurrence of such reverse mass-ordered systems.

Chapter 6

Conclusion

In this thesis, we explored the formation outcome of multi-planetary systems in inviscid disks. Using N-body code Rebound, we simulated the cores' initial short-lived disk-induced migration and the gravitational interaction between the cores that eventually lead to collisional mergers after the disk gas is largely dissipated. Our results show that the cores, especially the innermost ones, undergo some degree of inward radial drift at the level of $\lesssim$20% likely due to dynamical interaction with the outer planets. Our simulations further demonstrate that planetary systems that emerge from inviscid disks tend to be more stable against orbital instability and so merger events are rare as compared to what has been previously reported in viscous disks starting with different initial conditions. Identifying what the exact source of such stability is requires a more careful study. When the mergers happen, the core masses tend to become more similar to each other within a given system

as the innermost pairs merge first and sometimes the mergers are so vigorous that we end up with more massive objects at shorter orbital periods, which are currently not observed in the observations. Given the difficulty in detecting small and low mass planets at longer orbital periods, future ground-based instruments such as extreme precision radial velocity instruments at extremely large telescopes (ELT) and upcoming high precision space-based transit mission such as PLATO would be needed to definitively test our calculations.

Bibliography

Chiang, E., & Youdin, A. N. 2010, Annual Review of Earth and Planetary Sciences, 38, 493, doi: 10.1146/annurev-earth-040809-152513

Chiang, E. I., & Goldreich, P. 1997, ApJ, 490, 368, doi: 10.1086/304869

Dawson, R. I., Lee, E. J., & Chiang, E. 2016, ApJ, 822, 54, doi: 10.3847/0004-637X/822/1/54

Dong, R., & Fung, J. 2017, ApJ, 835, 146, doi: 10.3847/1538-4357/835/2/146

Dong, S., & Zhu, Z. 2013, ApJ, 778, 53, doi: 10.1088/0004-637X/778/1/53

Flaherty, K. M., Hughes, A. M., Rose, S. C., et al. 2017, ApJ, 843, 150, doi: 10.3847/1538-4357/aa79f9

Fressin, F., Torres, G., Charbonneau, D., et al. 2013, ApJ, 766, 81, doi: 10.1088/0004-637X/766/2/81

Fung, J., & Chiang, E. 2017, ApJ, 839, 100, doi: 10.3847/1538-4357/aa6934

Fung, J., & Lee, E. J. 2018, ApJ, 859, 126, doi: 10.3847/1538-4357/aabaf7

Funk, B., Wuchterl, G., Schwarz, R., Pilat-Lohinger, E., & Eggl, S. 2010, A&A, 516, A82, doi: 10.1051/0004-6361/200912698

Goldreich, P., & Tremaine, S. 1980, ApJ, 241, 425, doi: 10.1086/158356

Hayashi, C. 1981, Progress of Theoretical Physics Supplement, 70, 35, doi: 10.1143/PTPS.70.35

Hourigan, K., & Ward, W. R. 1984, Icarus, 60, 29, doi: 10.1016/0019-1035(84)90136-2

Howard, A. W., Marcy, G. W., Johnson, J. A., et al. 2010, Science, 330, 653, doi: 10.1126/science.1194854

Ida, S., & Lin, D. N. C. 2008, ApJ, 673, 487, doi: 10.1086/523754

Johansen, A., & Lambrechts, M. 2017, Annual Review of Earth and Planetary Sciences, 45, 359, doi: 10.1146/annurev-earth-063016-020226

Kanagawa, K. D., Tanaka, H., & Szuszkiewicz, E. 2018, ApJ, 861, 140, doi: 10.3847/1538-4357/aac8d9

Kley, W., & Nelson, R. P. 2012, ARA&A, 50, 211, doi: 10.1146/annurev-astro-081811-125523

Lambrechts, M., & Johansen, A. 2012, A&A, 544, A32, doi: 10.1051/0004-6361/201219127

Lambrechts, M., Johansen, A., & Morbidelli, A. 2014, A&A, 572, A35, doi: 10.1051/0004-6361/201423814

Laskar, J. 1997, A&A, 317, L75

Lee, E. J., & Chiang, E. 2016, ApJ, 817, 90, doi: 10.3847/0004-637X/817/2/90

Lin, D. N. C., & Papaloizou, J. C. B. 1993, in Protostars and Planets III, ed. E. H. Levy & J. I. Lunine, 749

MacDonald, M. G., Dawson, R. I., Morrison, S. J., Lee, E. J., & Khandelwal, A. 2020, ApJ, 891, 20, doi: 10.3847/1538-4357/ab6f04

Mamajek, E. E. 2009, in American Institute of Physics Conference Series, Vol. 1158, Exoplanets and Disks: Their Formation and Diversity, ed. T. Usuda, M. Tamura, & M. Ishii, 3–10

Mayor, M., & Queloz, D. 1995, Nature, 378, 355, doi: 10.1038/378355a0

Mayor, M., Marmier, M., Lovis, C., et al. 2011, arXiv e-prints, arXiv:1109.2497, doi: 10.48550/arXiv.1109.2497

Millholland, S., Wang, S., & Laughlin, G. 2017, ApJL, 849, L33, doi: 10.3847/2041-8213/aa9714

Mishra, L., Alibert, Y., Udry, S., & Mordasini, C. 2023, A&A, 670, A68, doi: 10.1051/0004-6361/202243751

NASA Exoplanet Archive. 2023, Planetary Systems, NExScI-Caltech/IPAC, doi: 10.26133/NEA12. https://catcopy.ipac.caltech.edu/dois/doi.php?id=10.26133/NEA12

Ormel, C. W. 2017, in Astrophysics and Space Science Library, Vol. 445, Formation, Evolution, and Dynamics of Young Solar Systems, ed. M. Pessah & O. Gressel, 197

Ormel, C. W., & Klahr, H. H. 2010, A&A, 520, A43, doi: 10.1051/0004-6361/201014903

Petigura, E. A., Howard, A. W., & Marcy, G. W. 2013, Proceedings of the National Academy of Science, 110, 19273, doi: 10.1073/pnas.1319909110

Petrovich, C., Deibert, E., & Wu, Y. 2019, AJ, 157, 180, doi: 10.3847/1538-3881/ab0e0a

Pinte, C., Dent, W. R. F., Ménard, F., et al. 2016, ApJ, 816, 25, doi: 10.3847/0004-637X/816/1/25

Pu, B., & Lai, D. 2019, MNRAS, 488, 3568, doi: 10.1093/mnras/stz1817

Pu, B., & Wu, Y. 2015, ApJ, 807, 44, doi: 10.1088/0004-637X/807/1/44

Rafikov, R. R. 2002, ApJ, 572, 566, doi: 10.1086/340228

Rein, H., & Liu, S. F. 2012, A&A, 537, A128, doi: 10.1051/0004-6361/201118085

Squire, J., & Hopkins, P. F. 2018, MNRAS, 477, 5011, doi: 10.1093/mnras/sty854

Tamayo, D., Rein, H., Shi, P., & Hernandez, D. M. 2020a, MNRAS, 491, 2885, doi: 10.1093/mnras/stz2870

Tamayo, D., Cranmer, M., Hadden, S., et al. 2020b, Proceedings of the National Academy of Science, 117, 18194, doi: 10.1073/pnas.2001258117

Ward, W. R. 1997, Icarus, 126, 261, doi: 10.1006/icar.1996.5647

Weiss, L. M., Marcy, G. W., Petigura, E. A., et al. 2018, AJ, 155, 48, doi: 10.3847/1538-3881/aa9ff6

Youdin, A. N., & Goodman, J. 2005, ApJ, 620, 459, doi: 10.1086/426895

Yu, C., Li, H., Li, S., Lubow, S. H., & Lin, D. N. C. 2010, ApJ, 712, 198, doi: 10.1088/0004-637X/712/1/198

Zhou, J.-L., Lin, D. N. C., & Sun, Y.-S. 2007, ApJ, 666, 423, doi: 10.1086/519918